

Heritability of nested hierarchical structural brain network

Moo K. Chung, Zhan Luo, Nagesh Adluru, Andrew L. Alexander, Richard J. Davidson, H. Hill Goldsmith

Abstract—When a brain network is constructed by an existing parcellation method, the topological structure of the network changes depending on the scale of the parcellation. To avoid the scale dependency, we propose to construct a nested hierarchical structural brain network by subdividing the existing parcellation hierarchically. The method is applied in diffusion tensor imaging study of 111 twins in characterizing the topology of the brain network. The genetic contribution of the whole brain structural connectivity is determined and shown to be robustly present over different network scales.

I. INTRODUCTION

In many brain connectivity studies, the whole brain is often parcellated into p disjoint 3D volumes, where p is usually 116 or less [15], [16]. Anatomical Automatic Labeling (AAL) is probably the most often used parcellation scheme for this purpose [15]. AAL parcellation provides 116 labels for cortical and subcortical structures (Figure 1) [15]. Subsequently, either functional or structural information is overlaid on top of AAL and $p \times p$ connectivity matrices that measure the strength of connectivity between brain regions are obtained. The major shortcoming of using the existing parcellations including AAL is the lack of refined spatial resolution. Even if we detect connectivity differences in large parcellations, it is not possible to localize what parts of parcellations are affected without additional analysis, which reduces the localization power and sensitivity.

Brain networks are fundamentally multiscale. Intuitive and palatable biological hypothesis is that brain networks are organized into *hierarchies* [1]. A brain network at any particular scale might be subdivided into subnetworks, which can be further subdivided into smaller subnetworks in an iterative fashion. Unfortunately, many existing hierarchical parcellation schemes give raise to conflicting topological structures from one scale to the next. The topological structure of parcellation at one particular scale may not carry over to different scales [16], [1]. Thus, there is a need to develop a hierarchical parcellation scheme that provide a consistent network analysis results regardless of the choice of scale.

In this paper, we propose a new nested hierarchical network using the *Courant nodal domain theorem* [6]. The proposed method is related to graph cuts [14] and spectral clustering [7], [13] based parcellation schemes previously used in parcellating the resting-state functional magnetic resonance imaging (fMRI). However, in all these studies, parcellations are not hierarchical or nested so they produce conflicting topology over different network scales. Unlike

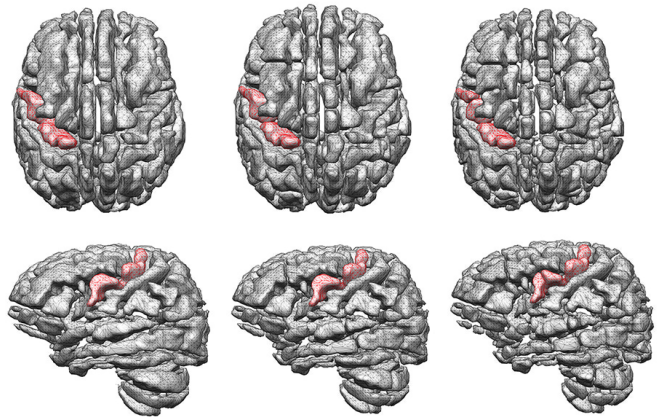


Fig. 1. Left: AAL parcellation with 116 regions. Each parcellation is displayed as a disconnected 3D volume. Red region is the left precentral gyrus. Middle: the second layer of the hierarchical parcellation with 2×116 regions. Each AAL parcellation is subdivided into two disjoint regions. Right: the third layer of the hierarchical parcellation with 4×116 regions.

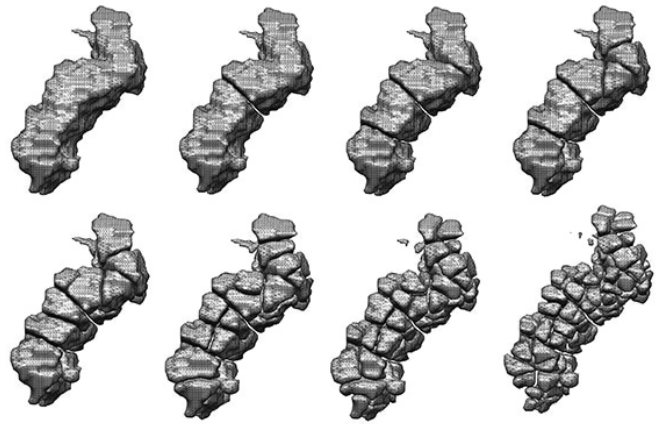


Fig. 2. Hierarchical parcellation of the left precentral gyrus shown in Figure 1 up to the 8-th layer. At the 8-th layer, we have $2^{8-1} = 128$ parcellations.

previous approaches, our proposed approach provides hierarchical nestedness and provide coherent topology across different spatial resolutions.

As an application, the proposed method was applied to diffusion weighted imaging (DWI) study of 111 twin pairs in determining the genetic contribution of topological properties of network topology.

II. HIERARCHICAL STRUCTURAL BRAIN NETWORK

A. Courant nodal domain theorem

For Laplacian Δ in a compact domain $\mathcal{M} \subset \mathbb{R}^3$, consider eigenvalues $0 = \lambda_0 < \lambda_1 \leq \lambda_2 \leq \dots$ and eigenfunctions

*The correspondence should be sent to mkchung@wisc.edu. All the authors are with University of Wisconsin, Madison, USA. This work was supported by NIH research grants R01 EB022856, R01 MH101504, P30 HD003352, U54 HD09025.

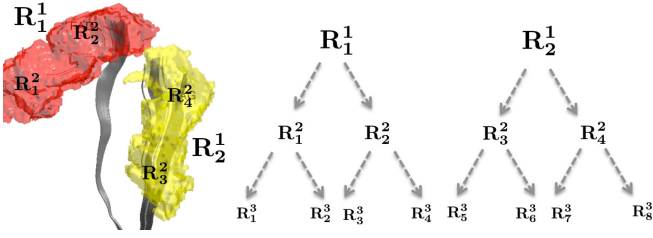


Fig. 3. Two representative AAL parcellations \mathbf{R}_1^1 (right precentral gyrus) and \mathbf{R}_2^1 (left precentral gyrus) at the first layer will be partitioned into four subregions $\mathbf{R}_1^2, \mathbf{R}_2^2, \mathbf{R}_3^2, \mathbf{R}_4^2$ at the second layer. The fiber tracts will be counted between the parcellations.

satisfying $\Delta\psi_j(p) = \lambda_j\psi_j(p)$. We then have $\psi_0(p) = 1/\sqrt{\mu(\mathcal{M})}$, where $\mu(\mathcal{M})$ is the volume of \mathcal{M} . From the orthogonality of eigenfunctions, we have

$$\int_{\mathcal{M}} \psi_0(p)\psi_1(p) d\mu(p) = 0,$$

Thus, ψ_1 must be take positive and negative values. The Courant nodal domain theorem [6], [4] further states that ψ_1 divides \mathcal{M} into two disjoint regions by the nodal surface boundary $\psi_1(p) = 0$. When the domain is discretized as a 3D graph, the second eigenfunction ψ_1 is called the *Fiedler vector*. Applying the nodal domain theorem iteratively, we can hierarchically partition \mathcal{M} in a nested fashion.

B. Hierarchical parcellation

We first convert the binary volume of each parcellation in AAL into a 3D graph by taking each voxel as a node and connecting neighboring voxels. Using the 18-connected neighbor scheme, we connect two voxels only if they touch each other on their faces or edges. This yields an adjacency matrix and the 3D graph Laplacian. The computed Fiedler vector is then used to partition each 3D AAL parcellation volume into two disjoint regions (Figures 2). This process continuous literately in subdividing a region into two smaller regions hierarchically. Since the number of voxels are not uniform across AAL parcellations, we are *approximately* doubling the number of parcellations at each iteration. There are total of $p = 116$ parcellations in layer 1 and $2 \cdot 116$ parcellations in layer 2. At layer 6, there are 3712 parcellations, which results in 61voxels per parcellation in average.

C. Hierarchical connectivity matrix

At the each layer of the hierarchical parcellation, we counted the total number of white matter fiber tracts connecting parcellations as a measure of connectivity. The resulting connectivity matrices form a hierarchically nested convolutional network. Let S_{jk}^i denote the total number of tracts between parcellations \mathbf{R}_j^i and \mathbf{R}_k^i at the i -th layer (Figure 3). The connectivity S_{jk}^i at the i -th layer is then the sum of connectivities at the $(i+1)$ -th layer (Figure 4), i.e.,

$$S_{jk}^i = \sum_{\mathbf{R}_l^{i+1} \subset \mathbf{R}_j^i} \sum_{\mathbf{R}_m^{i+1} \subset \mathbf{R}_k^i} S_{lm}^{i+1}.$$

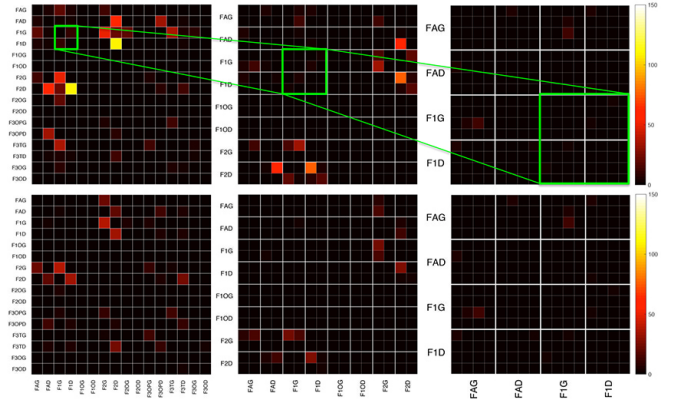


Fig. 4. The hierarchical connectivity matrices of MZ- (top) and DZ- (bottom). The parts of connectivity matrices of the layers 1, 2 and 3 are shown. They form a layered convolutional network, where the convolution is defined as the sum of tracts between sub-parcellations.

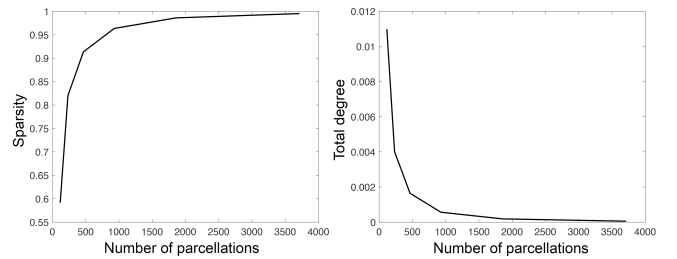


Fig. 5. Left: plot of sparsity over the number of pacellations. The sparsity is measures as the ratio of zero entries over all entries in the connectivity matrix. Right: plot of total degree of nodes over the number of pacellations. The vertical axis measures the ratio of the total number of connections over every possible connection. The plots all show the sparse nature of brain networks at any spatial scale.

The sum is taken over every subparcellation of \mathbf{R}_j^i and \mathbf{R}_k^i . This provide a subject-level connectivity matrix. The connectivity matrix $S^i = (S_{jk}^i)$ is expected to be very sparse at any scale (Figure 5). For 116×116 connectivity matrix, 60% of entries are zeros. As we increases the number of parcellations, the sparsity increases.

III. APPLICATION TO TWIN IMAGING STUDY

A. Subjects and image preprocessing

The method is applied to 111 twin pairs of diffusion weighted images (DWI) in determining the genetic contribution of structural brain networks. Participants were part of the Wisconsin Twin Project [9]. 58 monozygotic (MZ) and 53 same-sex dizygotic (DZ) twins were used in the analysis. Twins were scanned in a 3.0 Tesla GE Discovery MR750 scanner with a 32-channel receive-only head coil. Diffusion tensor imaging (DTI) was performed using a three-shell diffusion-weighted, spin-echo, echo-planar imaging sequence. A total of 6 non-DWI ($b=0$ s-mm²) and 63 DWI with non-collinear diffusion encoding directions were collected at $b=500, 800, 2000$ (9, 18, 36 directions). Other parameters were TR/TE = 8575/76.6 ms; parallel imaging; flip angle = 90°; isotropic 2mm resolution (128×128 matrix with 256 mm field-of-view).

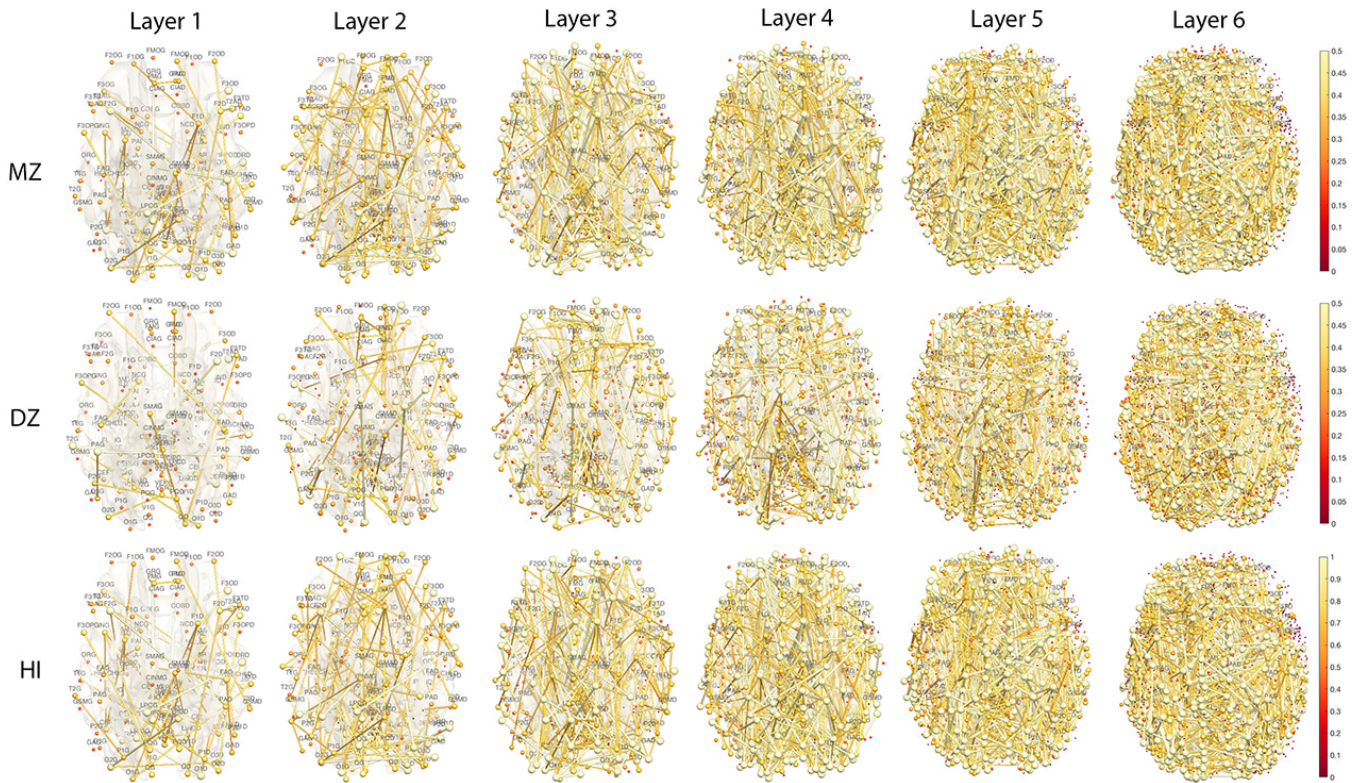


Fig. 6. Top, middle: Edge colors are Spearman’s rank correlations thresholded at 0.3 for MZ- and DZ-twins for different layers. Node colors are the maximum correlation of all the connecting edges. Bottom: Edge colors are the heritability index (HI). Node colors are the maximum HI of all the connecting edges. MZ-twins show higher correlations compared to DZ-twins. The node and edge sizes are proportionally scaled.

Image preprocessing follows the pipeline established in [3]. FSL were used to correct for eddy current related distortions, head motion and field inhomogeneity [10]. Estimation of the diffusion tensors at each voxel was performed using non-linear tensor estimation in CAMINO [11]. DTI-TK was used for constructing the study-specific template. Spatial normalization was performed for tensor-based white matter alignment using a non-parametric diffeomorphic registration method [17]. Each subject’s tractography was constructed using TEND algorithm, and tracts were terminated at FA-value less than 0.2 and deflection angle greater than 60 degree [12].

B. Heritability index

We are interested in knowing *the extent of the genetic influence on the structural brain network* and determining its statistical significance over different network scales. From the individual connectivity matrix which counts the number of tracts, we computed pairwise twin correlations. For discrete tract counts, it is more reasonable to use Spearman’s correlation than Pearson’s correlation. Note Spearman’s correlation is Pearson’s correlation between the sorted tract counts. Pearson’s correlation does not work well with discrete tract counts that often do not necessarily scale at the constant rate across different subjects and parcellations.

The twin correlations were used to compute the heritability index (HI) through Falconer’s formula, which determines the

amount of variation due to genetic influence in a population [8], [5]: MZ-twins share 100% of genes while DZ-twins share 50% of genes. The additive genetic factor A and the common environmental factor C are related as

$$\rho_{MZ} = A + C, \quad \rho_{DZ} = A/2 + C,$$

Thus, HI, as measured as A , is given by $HI = 2(\rho_{MZ} - \rho_{DZ})$, where ρ_{MZ} and ρ_{DZ} are the pairwise correlation between MZ- and same-sex DZ-twins (Figure 6).

C. Exact topological inference

We determined the statistical significance of MZ and DZ correlation network differences using the *exact topological inference* [5]. Let G_{λ}^{MZ} and G_{λ}^{DZ} be the binary networks obtained by thresholding ρ_{MZ} and ρ_{DZ} at correlation λ . Let B be a monotone graph function such that

$$B(G_{\lambda_1}^{MZ}) \leq B(G_{\lambda_2}^{MZ}) \quad \text{and} \quad B(G_{\lambda_1}^{DZ}) \leq B(G_{\lambda_2}^{DZ})$$

for $\lambda_1 \leq \lambda_2$ or $\lambda_1 \geq \lambda_2$. The number of connected components (Betti-0) and the total node degree are such functions. The test statistic

$$D_q = \sup_{1 \leq j \leq q} |B(G_{\lambda_j}^{MZ}) - B(G_{\lambda_j}^{DZ})|$$

is used to determine the statistical significance. The p -value under the null hypothesis of no network difference is then

given by [5]

$$P\left(D_q/\sqrt{2q} \geq d\right) = 2 \sum_{i=1}^{\infty} (-1)^{i-1} e^{-2i^2 d^2}.$$

D. Results

At each layer, we performed the exact topological inference. Figure 7 displays the change of the number of connected components (left), i.e., Betti-0 [5], and the total node degrees (right) over correlation values λ for MZ- (solid yellow) and DZ-twins (dotted red). The sudden topological changes are occurring at the almost same correlation values regardless of the scale of the network. This demonstrates the proposed hierarchical network is robust under scale change. The statistical significances are all less than 0.0002, 0.0002, 0.0002, 0.0002, 0.0002 and 0.0099 from layer 1 to 6 showing very strong and consistent overall genetic contribution of topological changes in the structural brain networks.

IV. DISCUSSION

We have developed a new nested hierarchical structural brain network method. The method was used in determining the genetic contribution of anatomical connectivity. The significance of genetic contribution has been reliably shown in many structural twin brain network studies [5], [2]. The different level of genetic makeup between MZ- and DZ-twins provides the fundamental basis for phenotypic brain variations. Thus the estimation of heritability provides a viable way evaluate the validity of our new network approach.

The proposed framework provides the topologically consistent statistical results regardless of the scale of the parcellation. Counting the number of fibers down to very small subregions raises the question if we have a sufficient density of streamlines to achieve robustness of the result. The use of Spearman correlation and supremum in the test statistic makes our approach very robust even in low streamline density. Since p -values are all below 0.0002 in layers 1 to 5, up to layer 5 seems to be robust enough for the method. With the proposed hierarchical network, we get much larger number of regions across the hierarchical scales than the number of subjects, which raise the problem of the ratio of feature dimensionality versus sample size. However, as our results demonstrated, we are still achieving the robust results.

Hierarchical parcellations are often proposed to determine the optimal level of scales and to explore across-scale similarities and invariants [16], [1], [14], [7], [13]. Statistics on finer levels may provide information on robustness and variability of human brain connectivity at these levels. We believe up to networks scales up to layer 5 (3712 parcellations) provides such robustness. It is hoped the proposed parcellation and network construction frameworks will provide more consistent and robust network analysis across different studies and populations without concern for spatial resolution.

REFERENCES

[1] R.F. Betzel and D.S. Bassett. Multi-scale brain networks. *Neuroimage*, 160:73–83, 2017.

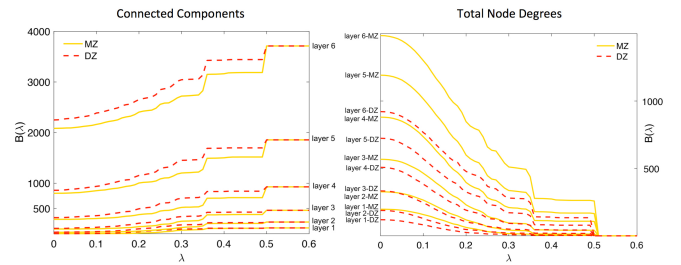


Fig. 7. Betti-0 plots. The number of connected components (vertical) over the thresholded correlation values (horizontal) at each layer. The plots scale up over different layers reasonably well. The sudden changes in the topological structure of network match up at the same correlation values.

[2] M.M. Bohlken, R.C.W. Mandl, R.M. Brouwer, M.P. van den Heuvel, A.M. Hedman, R.S. Kahn, and H.E.H. Pol. Heritability of structural brain network topology: a DTI study of 156 twins. *Human brain mapping*, 35:5295–5305, 2014.

[3] M.K. Chung, J.L. Hanson, L. Adluru, A.L. Alexander, R.J. Davidson, and S.D. Pollak. Integrative structural brain network analysis in diffusion tensor imaging. *Brain Connectivity*, 7:331–346, 2017.

[4] M.K. Chung, S. Seo, N. Adluru, and H.K. Vorperian. Hot spots conjecture and its application to modeling tubular structures. In *International Workshop on Machine Learning in Medical Imaging*, volume 7009, pages 225–232, 2011.

[5] M.K. Chung, V. Vilalta-Gil, H. Lee, P.J. Rathouz, B.B. Lahey, and D.H. Zald. Exact topological inference for paired brain networks via persistent homology. In *Information Processing in Medical Imaging (IPMI), Lecture Notes in Computer Science*, volume 10265, pages 299–310, 2017.

[6] R. Courant and D. Hilbert. *Methods of Mathematical Physics*. Interscience, New York, English edition, 1953.

[7] R.C. Craddock, G.A. James, P.E. Holtzheimer, X.P. Hu, and H.S. Mayberg. A whole brain fMRI atlas generated via spatially constrained spectral clustering. *Human Brain Mapping*, 33:1914–1928, 2012.

[8] D. Falconer and T Mackay. *Introduction to Quantitative Genetics, 4th ed.* Longman, 1995.

[9] H.H. Goldsmith, K. Lemery-Chalfant, N.L. Schmidt, C.L. Arneson, and C.K. Schmidt. Longitudinal analyses of affect, temperament, and childhood psychopathology. *Twin Research and Human Genetics*, 10:118–126, 2007.

[10] P. Jezzard and R.S. Balaban. Correction for geometric distortion in echo planar images from B0 field variations. *Magnetic Resonance in Medicine*, 34:65–73, 1995.

[11] D.K. Jones and P.J. Basser. Squashing peanuts and smashing pumpkins: How noise distorts diffusion-weighted MR data. *Magnetic Resonance in Medicine*, 52:979–993, 2004.

[12] M. Lazar, D.M. Weinstein, J.S. Tsuruda, K.M. Hasan, K. Arfanakis, M.E. Meyerand, B. Badie, H. Rowley, V. Haughton, A. Field, B. Witwer, and A.L. Alexander. White matter tractography using tensor deflection. *Human Brain Mapping*, 18:306–321, 2003.

[13] A. Pepe, G. Auzias, F. De Guio, F. Rousseau, D. Germanaud, J.-F. Mangin, N. Girard, O. Coulon, and J. Lefèvre. Spectral clustering based parcellation of fetal brain MRI. In *IEEE International Symposium on Biomedical Imaging (ISBI)*, pages 152–155, 2015.

[14] X. Shen, X. Papademetris, and R.T. Constable. Graph-theory based parcellation of functional subunits in the brain from resting-state fMRI data. *Neuroimage*, 50:1027–1035, 2010.

[15] N. Tzourio-Mazoyer, B. Landeau, D. Papathanassiou, F. Crivello, O. Etard, N. Delcroix, B. Mazoyer, and M. Joliot. Automated anatomical labeling of activations in spm using a macroscopic anatomical parcellation of the MNI MRI single-subject brain. *NeuroImage*, 15:273–289, 2002.

[16] A. Zalesky, A. Fornito, I.H. Harding, L. Cocchi, M. Yücel, C. Pantelis, and E.T. Bullmore. Whole-brain anatomical networks: Does the choice of nodes matter? *NeuroImage*, 50:970–983, 2010.

[17] H. Zhang, P.A. Yushkevich, D.C. Alexander, and J.C. Gee. Deformable registration of diffusion tensor MR images with explicit orientation optimization. *Medical Image Analysis*, 10:764–785, 2006.